Journal of the European Ceramic Society 13 (1994) 197–209

Failure Behaviour of Al_2O_3 with Glassy Phase at High Temperatures

T. Fett, M. Mißbach & D. Munz

Kernforschungszentrum Karlsruhe, Institut für Materialforschung II, Universität Karlsruhe, Institut für Zuverlässigkeit und Schadenskunde im Maschinenbau, Karlsruhe, Germany

(Received 9 April 1993; revised version received 28 October 1993; accepted 10 November 1993)

Abstract

The problem of lifetime predictions in the creep range of ceramics is studied for an alumina containing a glassy phase. Lifetime measurements are carried out at 1100 °C. Different ranges of lifetime characterised by failure due to subcritical crack growth and creep fracture can be identified. Lifetime predictions are performed on the basis of linear fracture mechanics (K concept) and based on creep crack growth (C^*, C(t) integrals). Whilst the predictions based on the C^* concept agree well with the measurements, the predictions with the C(t) integral extend over a larger range of lifetimes.

Das Problem der Lebensdauervorhersage im Kriechbereich von Keramiken wird für Aluminiumoxyd, das eine Glasphase enthält, untersucht. Die Lebensdauer wurde bei einer Temperatur von 1100 °C bestimmt. Es konnten verschiedene Bereiche in der Lebensdauer bestimmt werden, die durch ein unterkritisches Rißwachstum und Kriechbruch verursacht werden. Die Lebensdauervorhersagen wurden auf der Basis der linearen Bruchmechanik (K Konzept) und des Kriechbruchwachstums (C^*, C(t) Integral) durchgeführt. Während die Vorhersagen, basierend auf dem C^* Konzept, in guter Übereinstimmung mit den experimentellen Daten sind, ergeben die Vorhersagen, basierend auf dem C(t) Integral, eine zu lange Lebensdauer.

Le problème des prédictions de la durée de vie des céramiques sollicitées dans leur domaine de fluage a été étudié pour une alumine contenant une phase vitreuse. Les mesures de durée de vie ont été réalisées à 1100 °C. Différents domaines de durée de vie ont pu être identifiés, ils sont caractérisés par une rupture due à de la croissance sous critique ou par une fracture en fluage. Les prédictions de durée de vie ont été réalisées sur base de la mécanique linéaire de la rupture (concept de K) et sur base de la croissance de la fissure en fluage (C^*, intégrales C(t)). Les prédictions basées sur le concept C^* sont en accord avec les mesures, tandis que les prédictions effectuées à partir de l'intégrale C(t) couvrent un plus vaste domaine de durée de vie.

1 Introduction

At low temperatures the failure of ceramics can be described by the methods of linear elastic fracture mechanics. This allows lifetimes to be predicted for components exposed to any type of loading. However, at elevated temperatures, especially in the range of creep, the failure behaviour becomes a complex one.[1,2] Essentially, the following causes account for the failure of ceramic components in the high temperature range which may occur both individually and combined with each other:

- Spontaneous failure occurs when the stress applied attains or exceeds the strength.
- Fracture at elevated temperatures may be caused by subcritical crack propagation which starts from existing flaws. In the range of applicability of linear-elastic fracture mechanics the crack growth rate v is correlated with the stress intensity factor K_I and frequently a power law is obtained which applies to a wide range of velocities:[3]

$$v(K) = AK^N \qquad (1)$$

- In case of noticeable creep, creep induced deformation itself may lead to a failure limit if the function of a component is affected by an excessive global deformation.
- True failure, which is directly correlated with creep induced deformation, consists in creep rupture. This is the result of increasing internal damage which is accompanied by the formation

Journal of the European Ceramic Society 0955-2219/94/$7.00

and growth of pores. For metals, the experimental finding of failure due to creep is described by the Monkman–Grant relation according to which the product of minimum creep rate and lifetime is a constant

- In addition to creep-induced damage caused by the formation of pores the growth of existing cracks or of cracks developing during creep, e.g. by the coalescence of pores, should be taken into account, which growth can be studied using fracture mechanics methods. Whereas in the range of subcritical crack growth which can be described by linear-elastic fracture mechanics, the stress intensity factor was the stress variable at the crack, this is the C^* integral in the range of noticeable (secondary) creep.

  The rate of creep crack growth is expressed by[4]

$$v(C^*) = A_c (C^*)^{N_c} \qquad (2)$$

  The exponents N_c determined for this law are clearly smaller than the values typical of eqn (1) ($N \approx 10$)[5,6]

- A further failure mode in the high temperature range consists of oxidation, for which up to now no quantitative prediction of lifetime is possible.

It has been the goal of an experimental study made on Al_2O_3 containing a glassy phase to find out whether the lifetime can also be properly predicted by fracture mechanics methods in the zone of creep. One of the questions to be clarified has been up to which temperature levels and for which lifetime a prediction based on the K concept has to be used instead, into which the parameters of the creep law are integrated. Moreover, it was investigated whether, under conditions of creep, failure is caused solely by the growth of existing cracks or whether defects are newly formed as pores and micro-cracks. In that case it had to be examined whether the lifetime can be estimated using a creep fracture criterion.

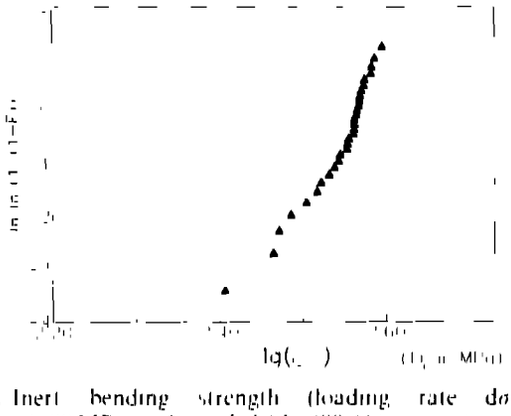

Fig. 1. Inert bending strength (loading rate $d\sigma/dt \approx$ 1500 MPa/s). Annealed 5 h, 900 °C (vacuum)

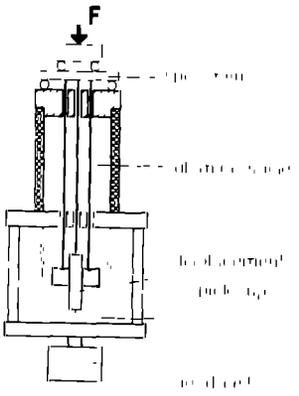

Fig. 2. Testing device for creep and lifetime tests

2 Material and Experimental Setup

Short characterisation of the material used.

- Inert strength (20 °C): Weibull parameters, $m = 16.5$, $\sigma_{0W} = 365$ MPa
- Fracture toughness: 20 °C: 3.4 MPa$\sqrt{m}$, 1100 °C: 4.1–5.2 MPa$\sqrt{m}$, 1200 °C: 3.1–5.0 MPa$\sqrt{m}$
- Elasticity data (20 °C): Young's modulus, $E = 325$ GPa, Poisson ratio, $\nu = 0.24$
- Further data: density 3.75 g/cm^3, mean grain size, 5 μm, composition: 96% Al_2O_3, 2.7% SiO_2, 1.3% MgO, 0.02% CaO, 0.02% Fe_2O_3

Bending specimens 3.5 × 4.5 × 45 mm were diamond machined and then annealed in vacuum for 5 h at 900 °C. Figure 1 shows inert bending data obtained in four point bending tests with a loading rate $d\sigma/dt = 1500$ MPa/s using a transient recorder. The Weibull parameters obtained with the maximum likelihood procedure are $m = 16.5$ and $\sigma_0 = 365$ MPa. Figure 2 illustrates the creep testing device used in the creep tests.[7] With this device the displacements can be measured within the inner roller span where the bending moment is constant.

3 High Temperature Behaviour

3.1 Creep behaviour

Figure 3 shows creep curves obtained at 1100 °C under different loads. The bending stresses noted in Fig. 3 are the elastically calculated outer fibre stresses. A pronounced primary creep range is obvious, which is followed by a nearly linear part caused by secondary creep.

The parameters of the creep law have to be determined from the strain time curves measured for different loads.

For an analytical representation of the creep law one can simply divide the creep strains ε_c into a primary component ε_p and a secondary component ε_s

$$\varepsilon_c = \varepsilon_p + \varepsilon_s \qquad (3)$$

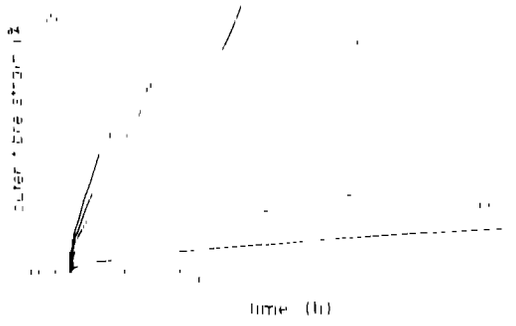

Fig. 3. Creep curves measured at 1100 C

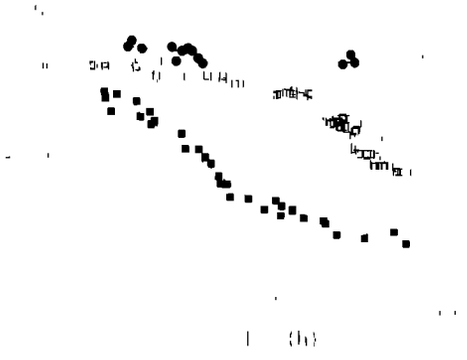

Fig. 4. Lifetimes measured in static four point bending tests

The secondary component is described by a modified Norton power law

$$\dot{\varepsilon}_s = D\chi_s|\sigma|^n$$

$$\chi_s = \begin{cases} 1 & \text{for } \sigma \geq 0 \\ -1 & \text{for } \sigma < 0, \quad \chi < 1 \end{cases} \qquad (4)$$

where the factor χ takes into consideration the non symmetric creep of ceramics containing a glassy phase. The primary creep behaviour is described by

$$\dot{\varepsilon}_p = C\sigma^m\varepsilon_p^{\ p} \qquad (5)$$

As a consequence of Bernoulli's hypothesis that plane cross sections remain plane during a bending test, the total strain ε composed of an elastic part and a creep part ε_c is a linear function of the distance from the centre line one can derive a differential equation that allows the stress and strain development in the bending bar to be determined[8]

$$\frac{\sigma}{E} = -\varepsilon_c + \frac{1}{2}\int_{-1}^{+1} \varepsilon_c \, d\eta + \frac{3}{2}\eta\int_{-1}^{+1} \varepsilon_c \, \eta \, d\eta \qquad (6)$$

where $\eta = 2y/H$ is the distance from the centre line normalised on half of the specimen height (H). The solution of this equation—which must be determined numerically in most cases—yields the time dependent stress distribution. On the other hand, the strains also result as a function of time. For any chosen set of unknown creep parameters a set of creep curves is obtained. The best set of parameters will then be obtained by use of a least squares procedure where the calculated and measured creep curves are systematically compared until a minimum in deviations is obtained. The procedure has been outlined in detail in Ref. 9. For the present Al_2O_3 ceramic the creep parameters were determined to be as shown in Table 1.

Table 1. Creep parameters at 1100 C

Primary creep	*Secondary creep*
$m = 4.8$	$n = 2.25$
$C = 1.3 \cdot 10^{-10}$ (MPa, h)	$D = 1.4 \cdot 10^{-8}$ (MPa, h)
$p = 2.1$	$\chi = 0.1$

It should be noted that it was possible to describe the tensile and compressive secondary creep with the same stress exponent n.

3.2 Lifetime measurements

Lifetime measurements were carried out in static four point bending tests with $3.5 \times 4.5 \times 45$ mm specimens at 1000, 1100 and 1200 C. From the results plotted in Fig. 4 an interesting stress dependency can be seen. The general features are described schematically in Fig. 5. For high initial bending stresses causing short lifetimes a flat curve with a strong influence of the stress on lifetimes is obtained (range I). With decreasing load applied, a steep curve follows, with the lifetimes much less stress sensitive (range II), and in the case of very low stress an increase in stress sensitivity can be stated (range III). At 1000 C only range I can be observed, whereas at 1200 C only the ranges II and III occur.

As suggested by Fig. 5, the nearly linear dependencies of $\log t_f$ on $\log \sigma_0$ suggest a power law relation

$$t_f \propto \sigma_0^{\ N} \qquad (7)$$

For the three regions the resulting exponents are entered in Table 2.

Since the lifetime tests were performed in a creep testing apparatus, it was also possible to measure the strains at failure. The result is given in Fig. 6 where the fracture strain is plotted as a function of the

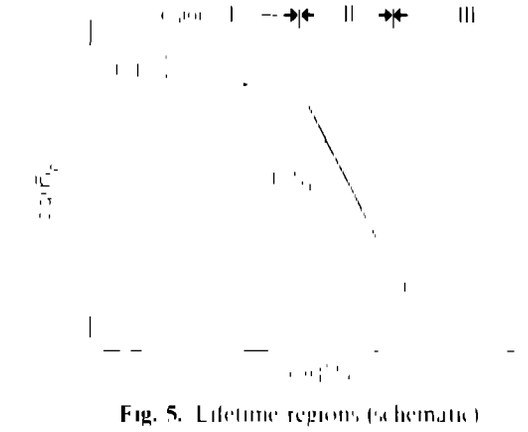

Fig. 5. Lifetime regions (schematic)

Table 2. Exponents of the stress-lifetime relation, eqn (7)

Temperature (°C)	N_I	N_{II}	N_{III}
1000	58.1		
1100	21.5	4.1	
1200		4.5	13.2

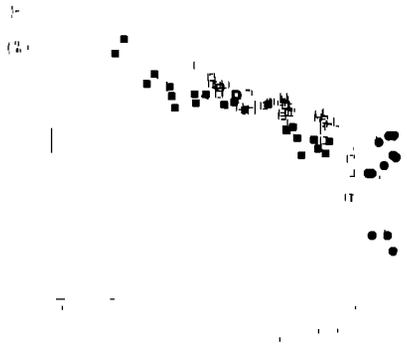

Fig. 6. Strains at failure for different temperatures ●, 1000 °C; □, 1100 °C; ■, 1200 °C

initially applied outer fibre bending stress σ_0. The strains at fracture decrease with increasing stress.

Figure 7 shows the minimum creep rates occurring in the secondary creep range, as a function of the lifetimes, for the tests at 1100 °C and 1200 °C. In the tests performed at 1000 °C no linear part of the creep curve and therefore no sufficiently constant value of the minimum creep rate have been obtained.

In the log–log representation of Fig. 7 a nearly linear dependency is found, i.e. a description

$$t_f \cdot \dot{\varepsilon}_{min}^{m} = \text{constant} \tag{8}$$

is possible. From the slopes which are identical with $-1/m$ one obtains $m = 1.4$ for 1100 °C and $m = 1.3$ for 1200 °C. A common representation of all data for both temperatures yields $m = 1.09$. The corresponding relation is entered in Fig. 7 as a dash dotted line. The slope of -1.09 is in good agreement with the Monkman–Grant relation,[10] which suggests a slope of -1. Consequently, the Monkman–Grant product is actually a constant.

In addition to the lifetime tests performed for

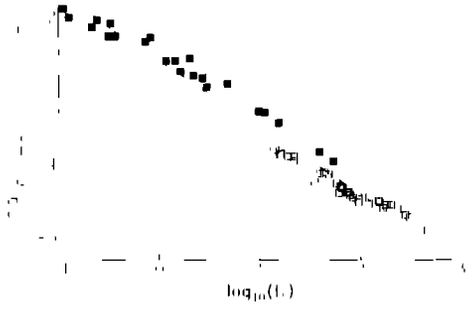

Fig. 7. Minimum creep rates in the secondary creep range □, 1100 °C; ■, 1200 °C

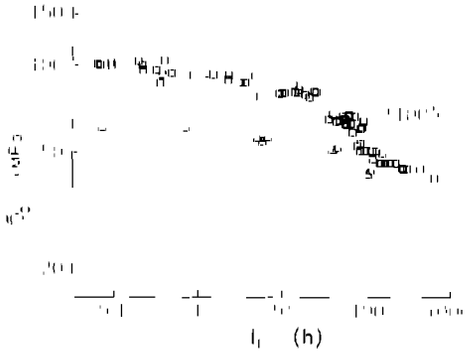

Fig. 8. Comparison of lifetimes for (□) natural cracks and (△) artificially introduced Knoop cracks

specimens with a natural flaw population tests with artificial surface cracks were also performed. In order to generate surface cracks, Knoop indentations were made on polished specimens and lifetime tests were carried out at 1100 °C with the cracked side positioned in the tensile region. In Fig. 8 the resulting lifetimes are compared with those obtained for the specimens with natural flaws.

In a number of tests the crack extension was measured. The initial crack width $2c$ was measured under the light microscope. Then the specimens were loaded at 1100 °C with 50 MPa bending stress and after periods of about 20 h the specimens were cooled down under load, the new crack width was measured and the test was continued. Results are represented in Fig. 9, which shows an increase in crack size after an incubation time of about 20 h.

3.3 Fracture-mechanical measurements

Creep induced crack growth describing the propagation of pre existing cracks or cracks generated during creep has very often been studied for metals, but investigations into ceramic materials are seldom.[5,6]

In the case of secondary creep the crack tip stresses are governed by the C^* integral, a path

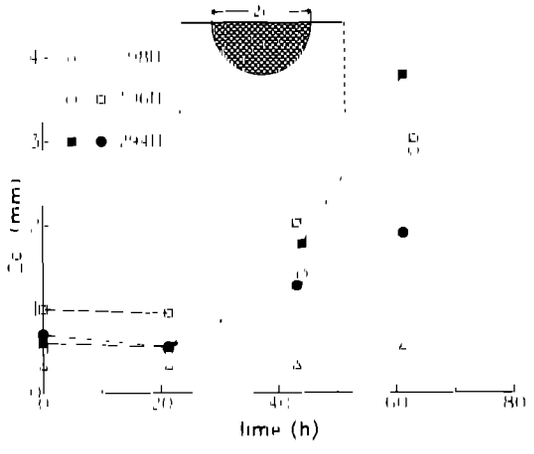

Fig. 9. Extension of Knoop induced surface cracks during static load tests at 1100 °C

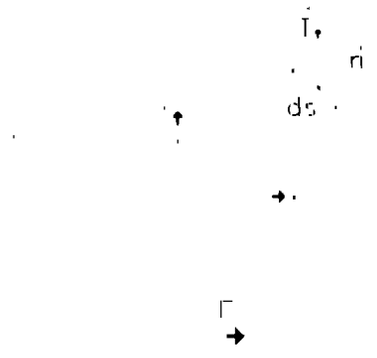

Fig. 10. Definition of the C^* integral

independent energy rate line integral which for one dimensional cracks (Fig. 10) is defined as

$$C^* = \int_\Gamma W^* \, dy - \mathbf{T}_i \frac{\partial \boldsymbol{\delta}_i}{\partial x} ds \qquad (9)$$

$$W^* = \int_0^{\dot{\varepsilon}_{ij}} \sigma_{ij} \, d\dot{\varepsilon}_{ij} \qquad (10)$$

where W^* is the strain energy density, $\mathbf{T}_i$ is the traction vector, $\boldsymbol{\delta}_i$ is the displacement vector, and ds is a line length increment along the contour Γ.

C^* governs the stresses and strains in front of a crack tip under steady state creep conditions[4].

In the creep power rate interpretation C^* can be expressed by the power difference of two identically loaded structures containing cracks of depths a and $a + da$, respectively, i.e.

$$C^* = -\frac{1}{B}\frac{dU^*}{da} \qquad U^* = \int_0^{\dot{u}} F \, du \qquad (11)$$

(B = specimen thickness). This relation offers the possibility to determine C^* experimentally. The quantities introduced in eqn (11) are explained in Fig. 11.

Equation (11) is the basis for a number of procedures used to determine C^*. A multiple specimen evaluation procedure based on dynamic bending tests performed with notched or pre-cracked bending bars at different displacement rates has been proposed by Landes & Begley[11]. The experimental input are the load–displacement curves for tests with very different displacement rates and the crack length data which are determined from partial unloadings. During the periodical partial unloadings the displacements are recorded. An example is shown in Fig. 12.

The slopes of the partial unloadings decrease with increasing crack length. During partial unloading and reloading hysteresis effects were observed. Therefore the usually applied compliance relation could not be applied. Dynamic bending tests were interrupted in different states and the specimens were broken at room temperature. Then it was possible to measure the crack size on the fracture surface and one point of the relation slope of the hysteresis = $f(a)$ has been determined. A series of such tests then yielded the complete calibration curve. The result of a single dynamic bending test performed with a bar containing a saw cut of 80 μm width and $a/t = 0.5$ undergoing a displacement rate $\dot{u} = 2$ μm h^{-1} is shown in Fig. 12(b). The crack starts

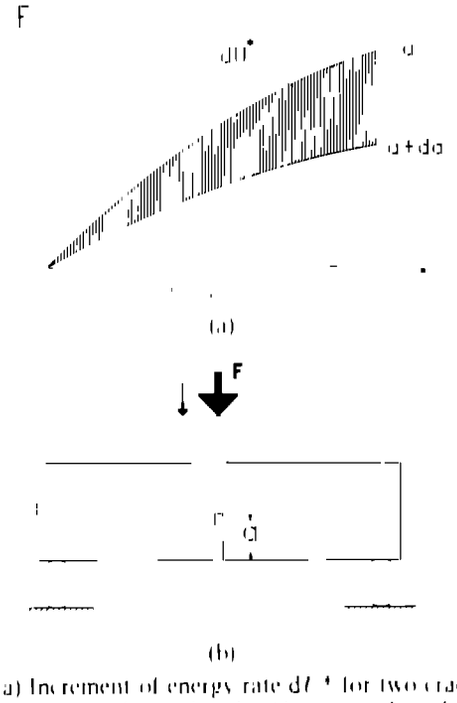

Fig. 11. (a) Increment of energy rate dU^* for two cracks with crack lengths a and $a + da$. (b) Geometrical and loading quantities.

Fig. 12. (a) Partial unloadings in a dynamic bending test. (b) Dynamic bending test performed to apply the procedure of Landes & Begley[11] (displacement rate 2 μm h^{-1}).

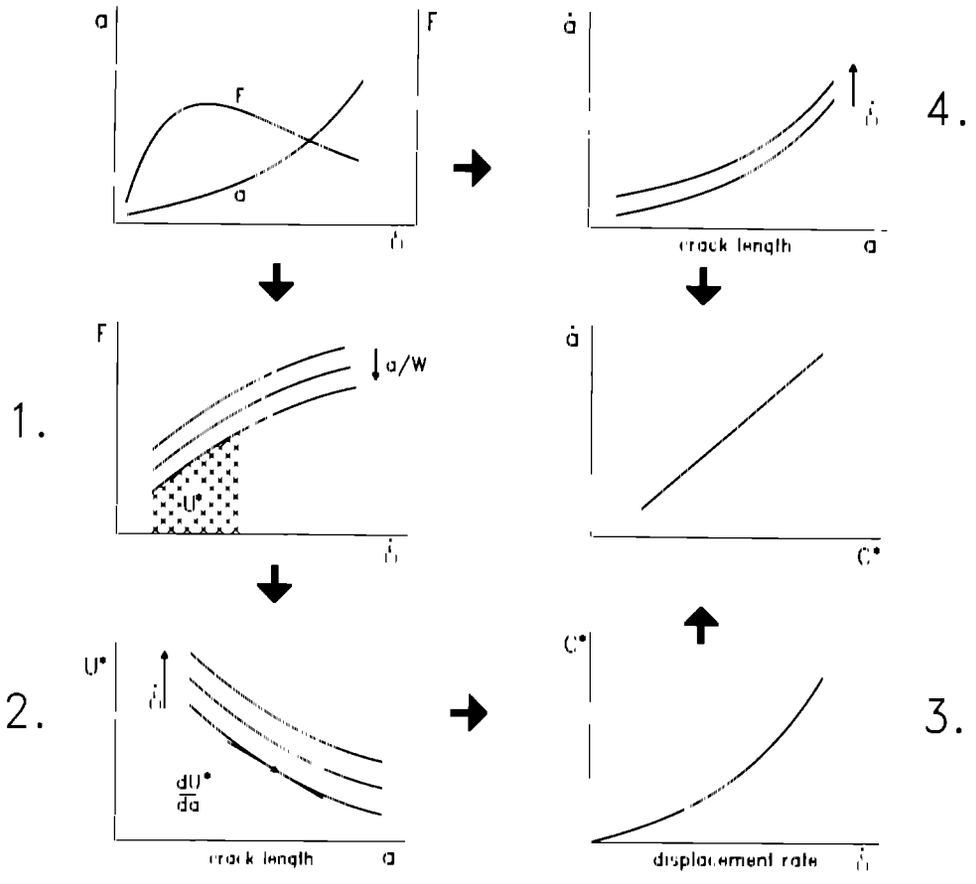

Fig. 13. The procedure of Landes & Begley[11] (schematic)

propagating approximately when the maximum load is reached and the following crack growth is nearly proportional to the time.

The procedure of Landes & Begley comprises several steps which are explained by the schematic representation in Fig. 13. The detailed description is given in the original paper [11]:

(1) In the first step the load F is plotted as a function of crack length a and displacement rate $\dot{\delta}$. The area below the resulting curves gives the energy rate $U^*(a,\dot{\delta})$.

(2) The representation $U^* = f(\dot{\delta}, a)$ provides the derivative $\partial U^*/\partial a$ as a function of $\dot{\delta}$.

(3) From eqn (11) C^* is calculated and plotted versus $\dot{\delta}$.

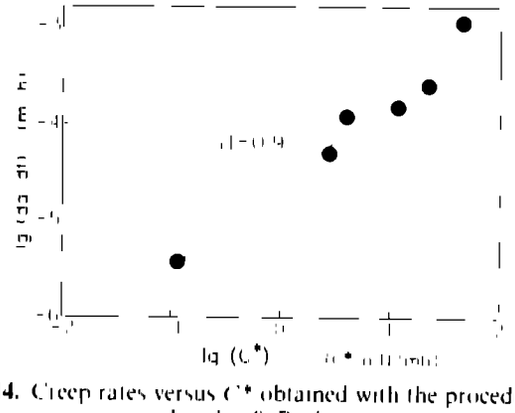

Fig. 14. Creep rates versus C^* obtained with the procedure of Landes & Begley

(4) The basic data directly give $da/dt = f(a,\dot{\delta})$ and, finally, the combination of steps 3 and 4 results in the da/dt versus C^* curve.

The final result of the procedure is plotted in Fig. 14 as a relation $da/dt - C^*$. A least squares fit yields

$$da/dt = 2.4 \cdot 10^{-5}(C^*)^{0.9} \quad (C^* \text{ in N/mh, } da/dt \text{ in m/h}) \quad (12)$$

with a relatively low crack growth exponent compared with the exponents of K controlled sub critical crack growth.

3.4 Some microscopic observations on creep cracks

Crack generation and crack development were investigated on some specimens with polished surfaces. The static bending tests were interrupted after fixed periods and the specimens were cooled down under load. Under the SEM the tensile region was searched for visible cracks and then the high temperature tests were continued. Figure 15 shows a sequence of photographs for one and the same location at three different times. Several cracks are visible. They follow appropriately oriented grain boundaries. Crack branching and intensive crack-surface interactions can be detected. In Fig. 15(b) one can see a broken grain boundary at an extremely large grain from which micro cracks start which end up as macro cracks. Figure 15(c) consists of two

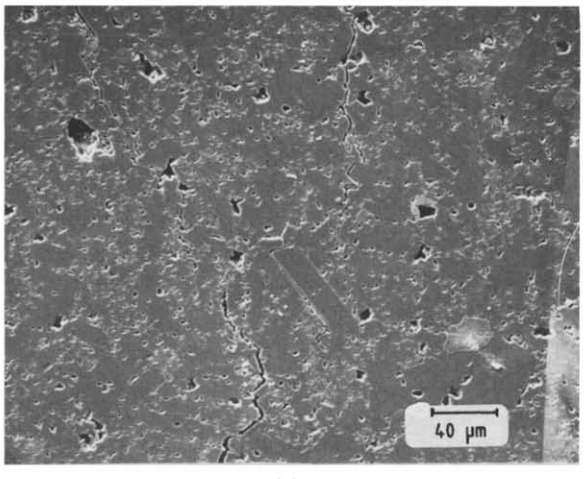

(a)

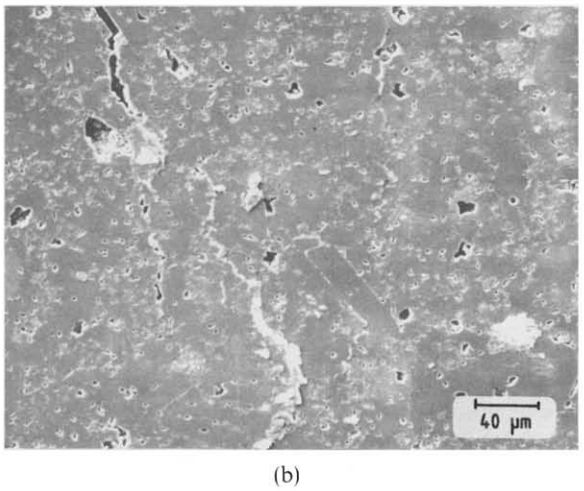

(b)

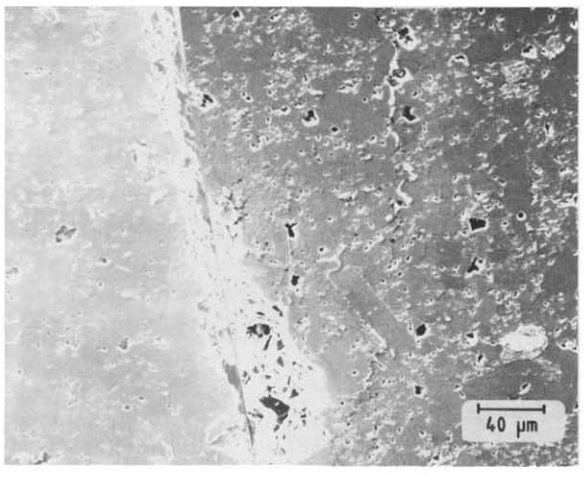

(c)

Fig 15 Creep crack in the tensile region of a bending bar loaded with $\sigma_0 = 60$ MPa (a) 84 (b) 136 and (c) 160 h

photographs of the broken specimen which have been joined together

A statistical evaluation of crack generation and crack development is given in Fig 16. On the polished tensile side of a bending bar a fixed surface area (Fig 16(a)) was inspected under the light microscope in order to detect surface cracks. To be made more visible the surface was painted with a mixture of coloured penetrating liquid and acetone

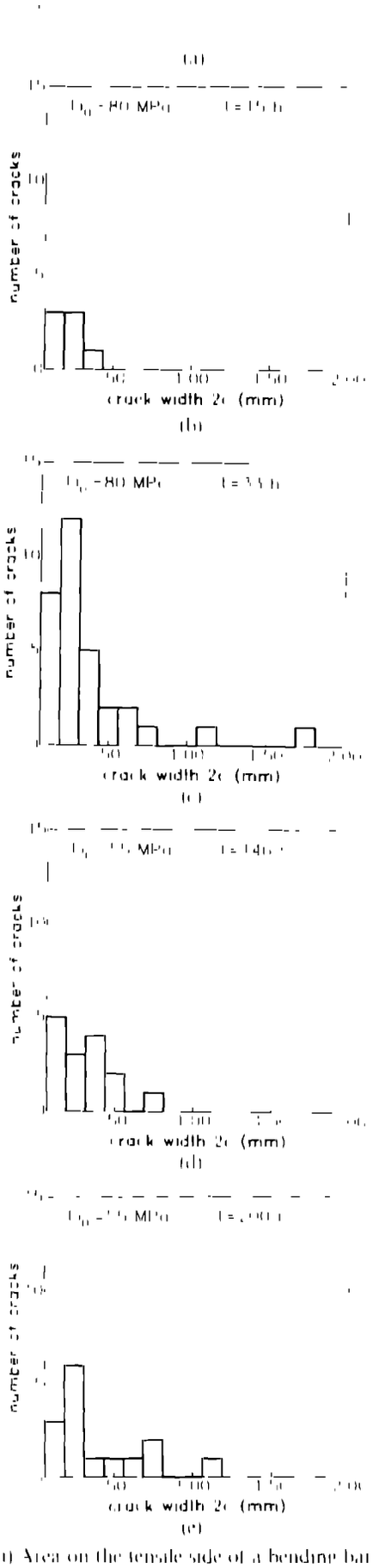

Fig 16 (a) Area on the tensile side of a bending bar inspected for creep cracks (b) (e) Size distribution of creep cracks

The crack sizes $2c$ were measured and divided into classes of 12.5 μm width. From Fig. 16(b)–(e) the generation (increase in the total crack number) and the propagation of cracks (shift of distribution to the right) becomes obvious.

4 Lifetime Predictions

Results of lifetime measurements in static bending tests have been reported in the experimental part. The resulting interdependency of the measured lifetimes (t_f) and the initial outer fibre bending stress (σ_0) showed an interesting behaviour. Three regions with significantly different slopes in the $\log(t_f)$ versus $\log(\sigma_0)$ plot have been identified. In order to understand this behaviour, predictions of the lifetimes were made on the basis of fracture mechanical concepts such as linear-elastic and creep fracture mechanics and on the Monkman-Grant relation which describes failure due to creep damage.

The fracture mechanical procedures require the stresses in the test specimens to be known. Since all creep parameters are known, from Section 2, the time dependent stresses can be computed according to eqn (6). The result is shown in Fig. 17. The elastic solution at the moment of loading ($t = 0$) gives a linear stress distribution with the initial outer fibre bending stress σ_0. With increasing time, the stresses become reduced at the tensile surface, and the neutral axis shifts to the compressive surface. Two regions are obvious where the stresses are nearly constant during the test. These regions are called 'skeleton points' independent of the fact that the curves fan out in reality.

4.1 Lifetime predictions using fracture-mechanical methods

The starting point are cracks or pores resembling cracks as can always be found in ceramic materials. The stresses around the crack tip which account for crack growth can be treated using the fracture mechanics concepts listed:

- Stress intensity factor K for linear-elastic material behaviour,
- J integral for elastic-plastic deformation,
- C integral for viscous behaviour.

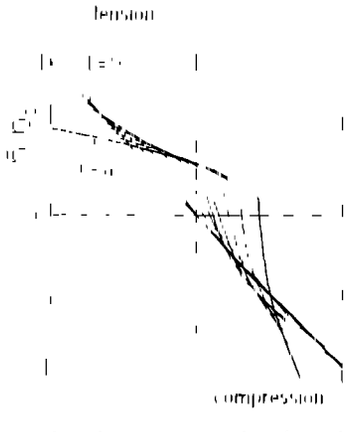

Fig. 17. Stress distribution in a bending bar under creep conditions.

4.1.1 Application of linear elastic fracture mechanics

The loading parameter of linear fracture mechanics is the stress intensity factor K which can be calculated from the crack size a, a characteristic stress σ, and the fracture mechanics geometry function Y:

$$K = \sigma \sqrt{\pi a}\, Y \tag{13}$$

This parameter controls subcritical crack growth in the range of application of linear-elastic fracture mechanics:

$$\frac{\mathrm{d}a}{\mathrm{d}t} = v(K) \tag{14}$$

For a number of ceramics a power law corresponding to eqn (1) applies in a large range of velocities. The lifetime of a loaded component then results simply from the integration of the crack growth law starting from an initial crack length a_i up to the critical value a_c:

$$t_f = \int_0^{t_f} \mathrm{d}t = \int_{a_i}^{a_c} \frac{\mathrm{d}a}{v(K)} \tag{15}$$

Failure occurs when the stress intensity factor attains the fracture toughness K_{Ic}, i.e. if

$$K = K_{Ic} \tag{16}$$

As has already been shown, the stress distribution in the creeping bending bar depends on the time. One possible treatment by fracture mechanics consists in the determination of stress intensity factors using the principle of superposition. For this, the stress distribution is approximated by an n-degree polynomial.

$$\sigma = \sum_{(n)} C_n \left(\frac{x}{W}\right)^n \tag{17}$$

As in the literature special stress intensity factors of stresses distributed according to a power law up to the degree $n = 5$ are available,[12] also the total stress intensity factor is known as a result of superposition:

$$K = \sigma \sqrt{\pi a} \sum_{(n)} C_n \left(\frac{a}{W}\right)^n Y_n \tag{18}$$

Due to the limited number of single solutions, this approach is restricted to stress distributions which

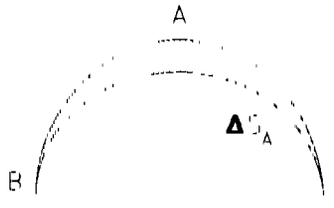

Fig. 18. Virtual crack increment ΔS_A

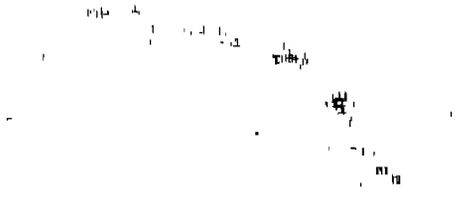

Fig. 20. Lifetimes of (—) Knoop damaged specimens predicted from the lifetimes of (□) specimens with natural crack population applying linear fracture mechanics

do not exhibit excessive variations. This applies above all to experiments conducted at high stresses. Because in that case the resulting lifetimes are only short and after these short periods the deviations from the linear initial distributions are still minor. Moreover, specimens fail under high loading at relatively small critical crack lengths.

In order to be able to determine stress intensity factors for any stress distributions using the weight function method (see e.g. synoptic representation[15]) suitably averaged stress intensity factors can be defined for semi-elliptical surface flaws. Physically meaningful averaging in which the local contributions of the energy release rates G are averaged has been proposed by Cruse & Besuner[14]. If G is the local energy release rate in a virtual enlargement by ΔS of the crack surface S, the total energy release rate taking into account $K^2 = GH$, reads

$$G_{\Delta S} = \frac{1}{\Delta S}\int_S G\,\mathrm{d}(\Delta S) = \frac{1}{H\Delta S}\int_S K^2\,\mathrm{d}(\Delta S) \qquad (19)$$

where $H = E$ for the case of plane stress and $H = E/(1-\nu^2)$ for the case of plane strain. The variable

$$K = \sqrt{G_{\Delta S}H} \qquad (20)$$

is now termed 'weighted averaged' stress intensity factor. It can be understood that after averaging of local stress intensity factors the average obtained must depend on the form of the virtual crack increment. To set a limit on the random approach Cruse & Besuner[14] proposed crack increments with two degrees of freedom for semi-elliptical surface cracks. The two crack increments have been represented in Figs 18 and 19.

With some experience accumulated, one can immediately see that the flat parts of the curves of the lifetime diagram (region I of Fig. 5) are indicating subcritical crack growth, whereas in the steep part (region II of Fig. 5) G- or K-driven creep crack growth is or at least might be the cause.

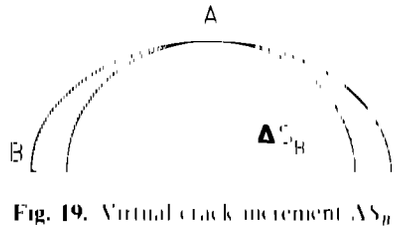

Fig. 19. Virtual crack increment ΔS_B

By integration of the power law the K driven crack growth can be calculated as a function of the time

$$\mathrm{d}a = AK_A^N\,\mathrm{d}t \qquad \mathrm{d}c = AK_B^N\,\mathrm{d}t \qquad (21)$$

The lifetime t_L is determined by the failure condition 'stress intensity factor = fracture toughness'. The data of the power law are obtained by adaptation to the lifetimes in the short term range. A mean crack depth of 84 μm was assumed which is obtained from the mean inert strength and the fracture toughness K_{Ic}. Introducing the time dependent stress distribution, the exponent $N = 10.9$ is obtained. This 'adapted' dependence on lifetime has been represented in Fig. 20 as a dash dotted curve. The finely dashed curves correspond to the minimum ($a_0 = 45\,\mu$m) and maximum ($a_0 = 109\,\mu$m) crack sizes which result from the maximum and minimum measured strength.

A first possibility of verification is offered by a simple relation which interlinks the Weibull parameters of lifetime m_L and strength m[1,16]

$$N = 2 + \frac{m}{m_L} \qquad (22)$$

From the Weibull parameter of the lifetimes of a constant stress level ($m_L = 1.78$ for $\sigma = 80$ MPa at 1100 °C) and the Weibull parameter of strength ($m = 16.5$, see Section 2) the exponent $N = 11.4$ is obtained in a good agreement with the adaptation of lifetime.

Additional measurements made on specimens with Knoop cracks have been evaluated as a second means of verification (Fig. 20). The crack growth law obtained with the natural cracks provides the prediction entered for the specimens with Knoop cracks. It is in excellent agreement with the experiment. This makes obvious that the short lifetimes are equivalent to a failure in conformity with the K concept.

4.1.2. The G concept

If the K concept applies predominantly to describe the linear elastic material behaviour, the G integral

must be used in cases of noticeable creep. The C^* integral can be calculated from the stress σ, the crack length a, and the parameters D, n of the Norton creep law. The following equation holds[4]

$$C^* = aD\sigma^{n+1}g(n, a/W) \tag{23}$$

The data available from the literature are not yet sufficient to determine the geometry function $g(a, n)$ for semi-circular and semi-elliptical surface cracks. However, the geometry function can be obtained in an approximation from the respective correction function of the K concept if $g(a, n)$ is known for a reference case[1-18]

$$\frac{C_1^*}{C_2^*} \approx \left(\frac{K_{I1}}{K_{I2}}\right)^2$$

and

$$\frac{g(a,n)_1}{g(a,n)_2} \approx \left(\frac{Y_1}{Y_2}\right)^2 \tag{24}$$

respectively.

The reference case used is the circular internal crack (penny shaped crack) whose geometry functions are known for K[19] and for C^*[20]

$$Y = \frac{2}{\sqrt{\pi}} \qquad g(a, n) = \frac{6}{\pi\sqrt{1 + 3n}} \tag{25}$$

With $n = 2.25$

$$g(a, n) = 0.98\,Y^2 \approx Y^2 \tag{26}$$

is obtained. Thus, the problem of determination of C^* can be reduced to the more familiar problem of stress intensity factor determination for any stress distributions.

In calculating the development of stress distribution versus time in a structure subjected to creep two very closely limited zones are mostly found, the skeleton points (solid circles in Fig. 21) where the stress, beginning at the moment of load application up to and including the steady state case, undergoes minor variations. As in the skeleton-point approximation all time-dependent stress curves occur between the two limit curves for $t = 0$ (elastic stress distribution) and $t \to \infty$ (asymptotic stress distribution), these two limit cases can be used to predict two limit cases of the lifetime under condition of creep crack growth between which the lifetime in the real experiment should lie. For the linear stress distribution the averaged stress intensity factors according to eqn (20) are represented by the geometric functions

$$Y_A = 1.92 - 0.914\beta + 0.173\beta^2 - 1.253\gamma + 5.306\gamma^2 - 2.19\gamma\beta - 4.652\gamma^2\beta + 1.954\gamma\beta^2$$

$$Y_B = 1.28 + 0.221\beta - 0.248\beta^2 - 0.024\gamma + 7.291\gamma^2 - 3.66\gamma\beta - 6.183\gamma^2\beta + 2.723\gamma\beta^2$$

and it results for the steady state stress distribution

$$Y_A = 1.92 - 0.908\beta + 0.168\beta^2 + 0.216\gamma + 6.418\gamma^2 - 2.97\gamma\beta - 5.694\gamma^2\beta + 2.276\gamma\beta^2$$

$$Y_B = 1.28 + 0.224\beta - 0.250\beta^2 + 0.645\gamma + 8.568\gamma^2 - 3.87\gamma\beta - 7.172\gamma^2\beta + 2.866\gamma^2\beta^2$$

with $\gamma = a/t$, $\beta = a/c$.

When the vertex belonging to the major axis of the ellipse gets close to the lateral specimen border a 'switch over' is effected from the semi-elliptical surface crack to the straight through crack having the same depth. The following relation can be obtained from Ref. 21 for through cracks under bending load

$$g(\gamma, n) = h_1(n, \gamma)\frac{(0.458n + 1)}{\gamma}(1 - \gamma)^{(2n+1)} \tag{27}$$

To facilitate use of the values h_1 tabulated in Ref. 21, they are fitted with respect to the relative crack depth γ and the Norton exponent n. The expression is obtained

$$h_1 = \gamma\left[1.26 + \sum_{\nu=1}^{4}\sum_{\mu=1}^{3} A_{\nu\mu}(1 - \gamma)^{\nu}n^{\mu-1}\right]^2 \tag{28}$$

with the coefficients

$A_{11} = 4.445$	$A_{23} = -9.312$	$A_{33} = -3.790$
$A_{12} = -4.552$	$A_{31} = 3.984$	$A_{41} = 13.543$
$A_{13} = 0.123$	$A_{32} = -23.267$	$A_{42} = -6.597$
$A_{21} = 8.908$	$A_{33} = 20.225$	$A_{43} = -1.333$

However, it should be recalled here that eqns (27) and (28) are applicable in an approximation only because the function h_1 had been determined to apply to materials exhibiting a symmetric deformation behaviour. However, these deviations are of minor importance to the lifetime prediction because the major part of the lifetime is 'consumed' in the

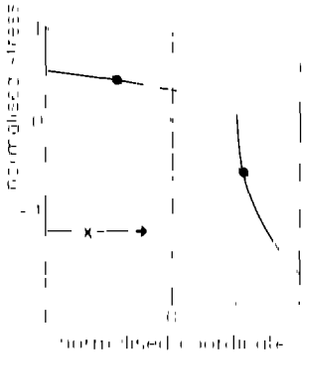

Fig. 21. Limit cases of the stress distribution establishing the skeleton points

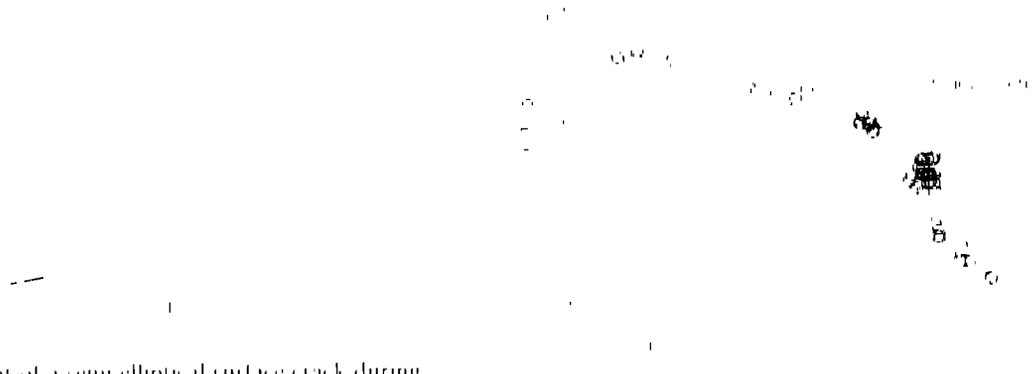

Fig. 22 Development of a semi elliptical surface crack during creep induced crack growth (solid curves: steady state stress distribution; dashed curves: calculated on the basis of the initial stress distribution); initial stress $\sigma_0 = 100$ MPa

Fig. 23 Lifetimes for bending load calculated by the C^* concept (1100 °C)

state characterised by the semi elliptical surface crack.

The crack growth rates developing in the range of creep can likewise be described by a power law (2), similar to K controlled subcritical crack growth. According to Riedel[4] the exponent is given by

$$N_c = \frac{n}{n+1} \tag{29}$$

which compared with the exponents of subcritical crack growth is rather small. The exponents are expected to be slightly less than unity. Especially for the material investigated it results from eqn (29) that with $n = 2.25$ $N_c = 0.7$. The value of N_c found in the creep crack growth experiments ($N_c = 0.9$, see eqn (9)) agrees well with the value obtained from eqn (29).

The crack growth parameter for the C^* concept was determined for 1100 °C in Section 2. The lifetime calculations based on these data include the numerical integration of the coupled system of differential equations

$$\mathrm{d}a = A_c(C^*_A)^{N_c}\,\mathrm{d}t \quad \mathrm{d}c = A_c(C^*_B)^{N_c}\,\mathrm{d}t \tag{30}$$

with the values A_c, N_c according to eqns (2) and (12). Figure 22 shows the development of an originally semi circular crack of depth $a = 50\,\mu$m as a function of the time up to the switch over point determined by

The dashed curves result from the linear initial stress distribution and the solid lines are based on the steady state stress distribution. It can be seen from the crack velocity at the moment of switch over which has much increased compared to that of the initial crack, that the corresponding time intervals are negligible. It is evident that the shape—a result of the low power of the crack growth law—remains nearly semi circular.

Lifetime calculations were performed for the two limit cases of stress. The result of prediction has been represented in Fig. 23 for the measurements made at 1100 °C. The authors started at a mean initial crack depth of 50 μm (corresponding to the inert strength and to K_{Ic}). The prediction on the left hand side is valid for the linear initial stress distribution, on the right hand side for the steady state stress. It can be easily recognised that due to eqns (2) and (29) the two limit curves describing the lifetime can be expressed by

$$t_f = \frac{1}{\sigma^{n-DN_c}} = \frac{1}{\sigma^{1.9375}} \tag{31}$$

i.e. the slope in the diagram $\log\sigma = f(\log t_f)$ is -1.2925. The actual lifetimes must occur between the two limit curves. Considering the good agreement of the calculated limit curves with the measured lifetimes, the conclusion can be drawn that in the steep range of lifetime curves failure calculated by the C^* concept must occur.

In addition, tensile tests were performed at 1100 °C.[11] The four values represented in Fig. 24 have been measured. Also for the experiments conducted under uniaxial tensile loading lifetime predictions were performed according to the C^* concept. In that special load case an analytical function can be indicated for the lifetime because of the nearly constant geometry function. With Y = constant = 1.28, integration of eqn (2) leads to

$$t_f = \frac{a_i^{1-N_c} - a_0^{1-N_c}}{(1-N_c)D^{N_c}\sigma^{(n+1)N_c}Y^{2N_c}A_c} \tag{32}$$

The elimination of the final crack length (a_f) which,

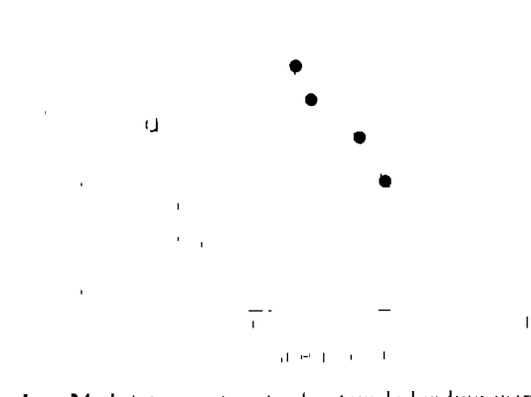

Fig. 24 Lifetime estimates for tensile loading using C^*

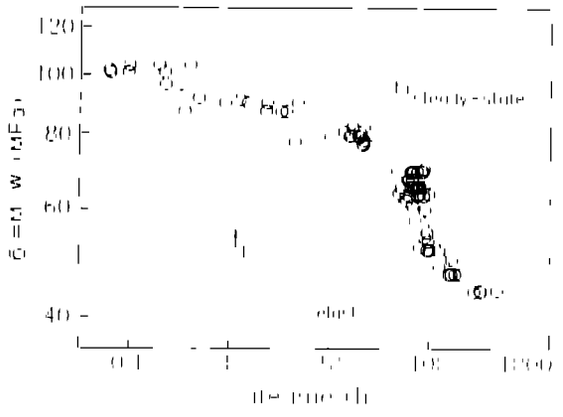

Fig. 25. Lifetimes for bending load calculated by the $C(t)$ concept (1100 °C)

due to the problematic fracture toughness K_{Ic} in the range of noticeable creep is not known, was dispensed with and a_c was considered to be a parameter. It appears from the calculation that this variable does not exert a marked influence on the lifetime. Figure 24 shows the predicted relationship between tensile stress and lifetime for a range of relevant final crack lengths as well as the values determined in the experiment.

Within the range of uncertainties caused by the final crack length which is not accurately known, an optimum agreement can be found between the prediction and the experiment.

4.1.3 Prediction based on the C(t) concept

For the application of the C^* concept it has to be taken into consideration that valid C^* values are obtained only after sufficiently long times t so that the condition of Riedel[4]

$$t \gg t_1 \quad t_1 = \frac{K^2(1-\nu^2)}{E(n+1)C^*} \tag{33}$$

is fulfilled in the tests. The characteristic time t_1 for the beginning of the lifetime test (i.e. calculated with the initial stresses) is entered in Fig. 25 as a dotted line. If the condition (33) is violated one has to use the $C(t)$ integral, which can be determined from Riedel's[4] interpolation formula

$$C(t) = \left(1 + \frac{t_1}{t}\right) C^* \tag{34}$$

Identical calculations as performed with the C^* integral were carried out with the $C(t)$ integral which replaced C^* in eqns (2) and (12). The numerical integration was started at a time $t_0 = 5$ s. During this time span, which is necessary for a smooth application of the bending load the creep crack state is undefined. Figure 25 shows the predictions based on the $C(t)$ concept. The two limit curves are shifted to lower lifetimes and only the limit curve resulting from the steady state stress distribution are in agreement with the measurements.

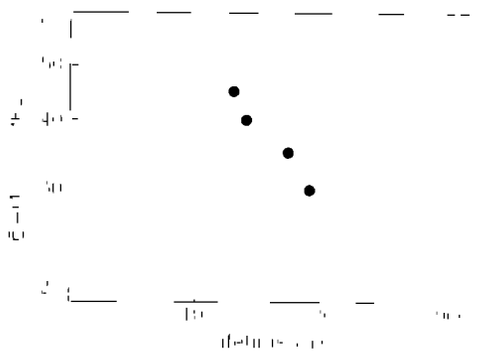

Fig. 26. Lifetime estimation for tensile loading according to Monkman & Grant[11]

4.2 Prediction according to Monkman Grant

To offer the complete variation of feasible predictions a prediction will be made here for creep induced fracture as the cause of failure. According to the Monkman-Grant relation, the product of the minimum creep rate and the lifetime is a constant. Figure 7 showed the dependence of the minimum creep strains on the lifetime. A straight line with a slope of approximately -1 could be recognised.

As all information about the Monkman-Grant product has been determined from values measured at the steep branch of the lifetime diagram, good agreement of a prediction with the bending tests is practically pre programmed.

Therefore, the creep rupture data obtained in the bending tests have been used to calculate the lifetimes in the four tensile creep tests. The dashed line in Fig. 26 shows the prediction according to the creep rupture concept. Also here a rather good agreement is obtained between the prediction and the measurement.

In conclusion, the question arises whether creep induced crack growth or creep rupture is responsible for the failure in the high temperature range. The study described makes evident that both causes taken together might account for failure. Additional microscopic pictures show that both existing cracks (e.g. Knoop cracks) grow and new cracks develop. This means that both effects are competing with each other.

5 Summary

The study related to the failure behaviour under static loading of Al_2O_3 containing glassy phases. By a comparison made between predictions on the basis of the

- K concept (subcritical crack growth),
- C^* and $C(t)$ concept (creep crack growth),
- Monkman-Grant relation (creep rupture)

predictions have been made. By a comparison with the experiments the range I, characterised by failure

due to subcritical crack growth, has been identified. The steep range II in the lifetime diagram can be described both by creep induced crack growth and by creep rupture.

Whilst the predictions based on the C^* concept agreed amazingly well with the measurements, the predictions with the $C(t)$ integral extend over a larger range of lifetimes.

Taking into consideration the agreement of the different types of predictions with the measured lifetimes and the microscopic findings it seems obvious that in the long lifetime range both effects compete with each other.

Acknowledgement

The financial support of the Deutsche Forschungsgemeinschaft is gratefully acknowledged.

References

1. Grathwohl G. Regimes of creep and slow crack growth in high temperature rupture of hot pressed silicon nitride. In *Deformation of Ceramics II*. Plenum Publishing Corporation 1984 pp. 573–86.
2. Quinn G. D. In *Ceramic Materials and Components for Engines*, ed. W. Bunk & H. Hausner. Verlag Deutsche Keramische Gesellschaft, Bad Honnef, Germany, 1986 pp. 931–00.
3. Fett T., Keller K. & Munz D. Determination of c–K curves of hot pressed silicon nitride at elevated temperatures. *Int. J. Fract.* **36** (1988) 3–14.
4. Riedel H. *Fracture at High Temperatures*. Springer Verlag, Berlin, 1987.
5. Kromp K., Haug T., Pabst R. F. & Gerold V. 'K_{Ic} for ceramic materials?' In *Third Conference on Creep and Fracture of Engineering Materials and Structures*. London 1989 pp. 1021–30.
6. Martin G., Fett T. & Munz D. Determination of creep crack growth in ceramics. In *Proc. 2nd ECRS Conference*, Augsburg, 1991.
7. Fett T., Keller K. & Rosenfelder O. German Patent 3629131 C2.
8. Fett T., Keller K. & Munz D. An analysis of the creep of hot pressed silicon nitride in bending. *J. Mater. Sci.* **23** (1988) 467–74.
9. Fett T., Keller K., Mißbach M., Munz D. & Pintschovius L. Creep parameters of alumina containing a glass phase determined in bending creep tests. *J. Amer. Ceram. Soc.* **71** (1988) 1046–9.
10. Monkman F. C. & Grant N. J. An empirical relationship between rupture life and minimum creep rate in creep-rupture tests. *Proc. ASTM* **56** (1956) 593–620.
11. Landes J. D. & Begley J. A. ASTM STP 590, 1976, pp. 128–48.
12. Fett T., Munz D. & Neumann I. Local stress intensity factor for surface cracks in plates under power shaped stress distributions. *Engng. Fract. Mech.* **36** (1990) 647–51.
13. Fett T., Matthieck C. & Munz D. Approximate weight function for 2D and 3D problems. *Engng. Anal. Boundary Elements* **6** (1989) 48–63.
14. Cruse T. A. & Besuner P. M. *J. Aircraft* (1975) 369–75.
15. Evans A. G. & Wiederhorn S. M. Proof testing of ceramic materials—an analytical basis for failure prediction. *Int. J. Fract.* **10** (1974) 379–92.
16. Ritter J. E. Engineering design and fatigue failure of brittle materials. In *Fracture Mechanics of Ceramics II*. Plenum Press, 1978, pp. 667–86.
17. Ainsworth R. A. Some observations on creep crack growth. *Int. J. Fract.* **20** (1982) 147–59.
18. Ainsworth R. A., Chell G. G., Coleman M. C., Goodall I. W., Gooch D. J., Haigh J. R., Kimmins S. T. & Neate G. J. CEGB assessment procedure for defects in plant operating in the creep range. *Eur. Struct. Integrity Mat. Str.* **10** (1987) 11–25.
19. Tada H. *The Stress Analysis of Cracks Handbook*. Del Research Corporation, 1986.
20. He M. Y. & Hutchinson J. W. The penny-shaped crack and the plane strain crack in an infinite body of power-law material. *ASME Trans.* **48** (1981) 830–40.
21. Kumar V., German M. D. & Shih C. F. An engineering approach for elastic-plastic failure analysis. EPRI Report NP-1931, Palo Alto, 1981.
22. Guttler M. Entwicklung einer Zugkriechapparatur für Hochlerntemperaturkeramiken und Zugkriechuntersuchungen an Siliziumnitridwerkstoffen. KfK Bericht 4874, Karlsruhe, May 1991.